Multi-band infrared detector assemblies and performances for 2nd-generation GEO meteorological satellite

Liu Dafu[1,2], Xu Qinfei[1,2,3], Wang Yang[1,2], Jia Jia[1,2], Yuan Honghui[1,2]

(1. State Key Laboratories of Transducer Technology, Shanghai Institute of Technical Physics, Chinese Academy of Sciences, Shanghai 200083, China;
2. Key Laboratory of Infrared Imaging Materials and Detectors, Shanghai Institute of Technical Physics, Chinese Academy of Sciences, Shanghai 200083, China;
3. University of Chinese Academy of Sciences, Beijing 100049, China)

Abstract: The second-generation geostationary orbit (GEO) quantitative remote sensing meteorological satellite had been developed by China. Channels of the satellite's scanning radiometer are increased from four of 1st generation Fengyun-2 to fourteen, with eight infrared channels covering the infrared band from short band to very long band. The eight infrared bands are implemented by three assemblies, known as shortwave dual channel assembly (MS-IR), water vapor dual channel assembly (WV-IR) and long wave four-channel assembly (LW-IR). The MS-IR contains two 8 × 1 PV MCT detector chips, corresponding to two CMOS low-temperature amplifiers, to achieve the photoelectric voltage signal conversion and amplification. The WV-IR contains two 4×1 MCT detector chips. LW-IR contains two 4 ×1 and one 4×2 MCT detector chip. These assemblies have good electrical and optical properties, such as MS-IR D^* is up to 1×10^{12} cm·Hz$^{1/2}$·W^{-1}. WV-IR D^* is better than 8×10^{10} cm·Hz$^{1/2}$·W^{-1}. The response spectra of these eight bands are quantitatively controlled, and the response spectrum is limited to the inner and outer limits. The small spot scanning system test results show that there was no obvious optical crosstalk inside the assembly. The registration accuracies between the two bands were better than 0.01 mm. In this paper, these assemblies are described, as well as performance, such as electrical performance, chip registration, optical crosstalk and relative spectral response.

Key words: GEO meteorological satellite; infrared detector assembly; slit scanning; spectral quantification; stray light; cross talk

CLC number: TN215 **Document code:** A **DOI:** 10.3788/IRLA201847.0404007

第二代静止轨道气象卫星用多波段红外探测器封装及性能

刘大福[1,2],徐勤飞[1,2,3],汪 洋[1,2],贾 嘉[1,2],袁洪辉[1,2]

(1. 中国科学院上海技术物理研究所 传感技术联合国家重点实验室,上海 200083;
2. 中国科学院上海技术物理研究所 红外成像材料与器件重点实验室,上海 200083;
3. 中国科学院大学, 北京 100049)

收稿日期:2017-10-10; **修订日期**:2017-11-20

基金项目:民用航天技术预先研究项目

作者简介:刘大福(1979-),男,研究员,主要从事光电探测器方面的研究。 Email: liudafu@mail.sitp.ac.cn

摘 要:第二代地球静止轨道(GEO)气象卫星用于定量化气象预报,中国已经成功研制出该卫星。卫星上扫描辐射计的探测波段从第一代风云二号的四个增加到现在的十四个,十四个波段中有八个是红外波段,覆盖了短波到甚长波的红外波段。这八个红外波段由三个组件来实现,分别是短波双波段组件(MS-IR),水汽双波段组件(WV-IR)和长波四波段组件(LW-IR)。 MS-IR 组件内包含两个 8×1 光伏型的 MCT 探测器芯片, 及相对应的两个用于光电输出的电压信号转换和放大的 CMOS 低温放大器。 WV-IR 包含两个 4×1 MCT 探测器芯片。 LW-IR 包含两个 4×1 和一个 4×2 MCT 探测器芯片。这些组件具有较高的电学和光学特性,如 MS-IR 的 D^* 可达 1×10^{12} cmHz$^{1/2}$ W^{-1}。 WV-IR 的 D^* 优于 8×10^{10} cm·Hz$^{1/2}$ W^{-1}。这八个波段的响应谱均实现了定量化控制,即响应谱控制在给定的内部和外部限制边内。对组件进行了狭缝扫描测试,结果表明组件内部没有明显的光学串扰。没两个波段间的配准精度优于 0.01 mm。文中描述了这些组件的结构以及达到的性能,如电性能,芯片配准,光学串扰和光谱响应。

关键词: GEO 气象卫星; 红外探测器封装; 狭缝扫描 ; 光谱定量化; 杂散光; 串音

0 Introduction

The second-generation geostationary orbit (GEO) quantitative remote sensing meteorological satellite had been developed by China. The radiation imaging channel of satellite is increased from Fengyun-2′s 5 to 14 [1], covering the visible, near infrared, short wave infrared, medium wave infrared and long wave infrared bands. Therefore, radiometer of the satellite can not only observe the cloud, water vapor, vegetation, earth surface, but also to capture aerosols and snow, and can distinguish different phases of clouds, high and middle water vapor.

There are eight infrared bands in the multi-channel scanning imaging radiator[2-3]. The infrared bands are realized by three infrared assemblies. Two wavelength bands of 2.1-2.35 μm and 3.5-4.0 μm are photovoltaic (PV) type detector, encapsulated in the short-wave dual-channel assembly (MS-IR). Two wavelength bands of 5.8-6.7 μm, 6.9-7.3 μm are photoconductive (PC) type detector, encapsulated in the water vapor dual-channel assembly (WV-IR). 8.0-9.0 μm, 10.3-11.3 μm, 11.5-12.5 μm and 13.2-13.8 μm are encapsulated in the long wave four-channel assembly (LW-IR). Table 1 shows the configuration of the three assemblies.

Tab.1 Parameters of the detector bands

Assembly	Wavelength/μm	Band symbol	Pixel	Size	Type
MS-IR	2.1-2.35	MS-B	56 μm×56 μm	8×1	PV
	3.5-4.0	MS-A	56 μm×56 μm	8×1	PV
WV-IR	5.8-6.3	WV-B	56 μm×56 μm	4×1	PC
	6.9-7.3	WV-A	56 μm×56 μm	4×1	PC
LW-IR	8.0-9.0	LW-D	56 μm×56 μm	4×1	PC
	10.3-11.3	LW-C	5656 μm×56	4×1	PC
	11.5-12.5	LW-B	56 μm×56 μm	4×1	PC
	13.2-13.8	LW-A	56 μm×56 μm	4×1	PC

1 Assembly structure

Pixel of the medium and short wavelength bands is 56 μm×56 μm, and each chip has eight pixels arranged in the manner shown in Fig.1 (a). The pixel of the other six bands is also 56 μm × 56 μm as shown in Fig.1(b).

The assemblies are packaged in a metal shell that incorporates chips, infrared filters, lens and apertures. There are two lenses in each assembly called lens *A* and lens *B* respectively.

There is an aperture closed to the detector chip, called 2nd aperture. On its top is another aperture called 1st aperture. The distance between two apertures is about 1 mm. These two apertures are used to suppress stray light in the shell. The filters are located on the 2nd aperture. The

electrodes of the chip are connected to the outside of the assembly by means of an electrode plate made of a sapphire material. Two lenses are installed in the lens base, through precision machining and clearance with ±0.02 mm positioning accuracy and 0.05 mm axis deviation positioning. Figure 2 is a schematic diagram of the assembly.

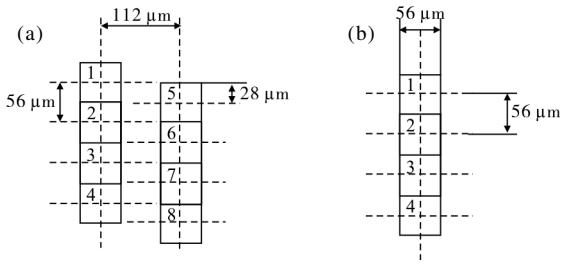

Fig.1 Pixel layout of (a)PV pixel, (b)PC pixel

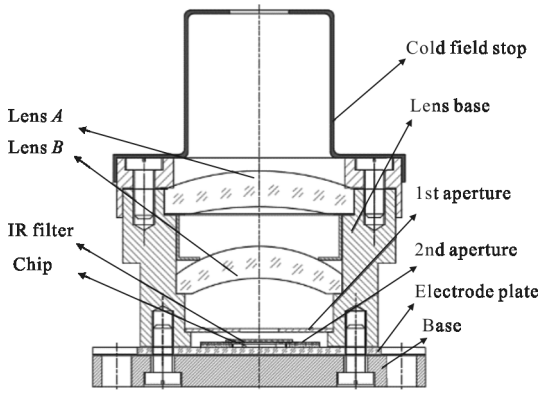

Fig.2 Diagram of the assembly structure

The photo-generated current signals of middle-wave and short-wave chips in MS-IR are amplified and converted to voltage signals by two low-temperature amplifiers, which are negative feedback amplifiers as shown in Fig.3. Figure 4 is the relationship of feedback resistance and temperature.

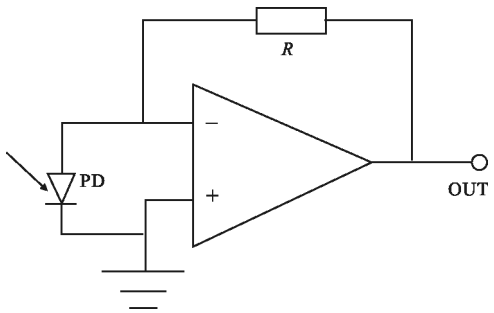

Fig.3 Schematic diagram of the low temperature amplifier

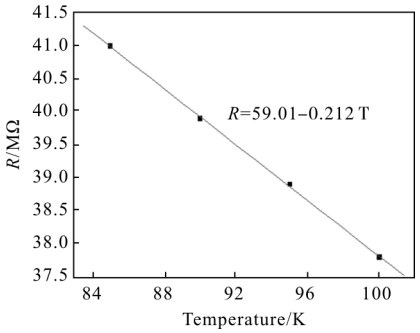

Fig.4 Feedback resistance vs temperature of the low temperature amplifier

2 Stray light suppression in the assemblies

Remote sensing detection system, especially the remote obs ervation of the infrared remote sensing optical system, is susceptible to stray light interference, such as the sun and the earth′s radiation, and stray light suppression has been one of key technology in remote sensing system [3]. Because infrared assembly is one of the core component in the system, the stray light in them is not only the matter the remote sensing system care about, but also the focus of the assembly designers pay attention to.

The source of stray light in the module is multifaceted and it is related to the factors such as the detector chip, the surface treatment of the package parts, the arrangement of the optical elements, the structure and size, etc. All of these may cause the non-imaging light coming into the surface of the detectors. Surface treatments of assembly parts must be done to reduce the specular reflection and improve the infrared absorption ability, such as blackening on the surface of the aperture and the field diaphragm. Crosstalk or MTF is usually used to quantitatively evaluate the stray light suppression effect in infrared assemblies.

Each assembly in the three assemblies of the radiometer contain more than one band, so in

addition to considering the stray light from the parts surfaces, that from the different bands should also be considered. Figure 5 shows the chip space between the chip and the distance between the chips and the filters, it can be seen that the minimum center distance between the different wavelengths of the pixel is only 512 μm, the distances between filters and chips are 300–500 μm. In this case, the optical crosstalk between such small distances will be one of the most importance that potentially cause stray light.

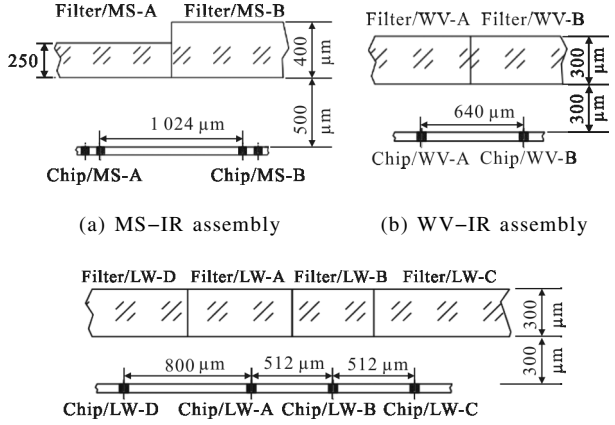

(a) MS–IR assembly (b) WV–IR assembly

(c) LW–IR assembly

Fig.5 Chip pixel and filter layout

As shown in Fig.6(a), the incident rays of the two bands *A* and *B* are incident on the *A* and *B* pixels through the filters *A* and *B* respectively, and this is an ideal state. It will not produce light cross–talk. When the light transmission direction is as shown in Fig.6 (b), a beam of light from the *A*–band filter incident, irradiation to the *A* pixel, and then the beam is reflected by chips and filters, then arriving at *B* pixel, finally causing *B* pixel to produce an optical signal, thereby producing an optical cross–talk. The case of Fig.6(c) is similar to that of Fig.6 (b), except that the light beam of Fig.6(c) enters from the upper surface of the *A* filter and then passes through the lower surface of the *B* filter, and finally passes through a series of reflections, transmitted to the detector pixel, causing stray light. Figure 6 (d) shows that the incident beam transmitted from the *A* filter into the filter substrate and then reflected or transmitted through the upper and lower surface, then the beam transmits into the right side of the filter, finally the beam reaches *B* pixel.

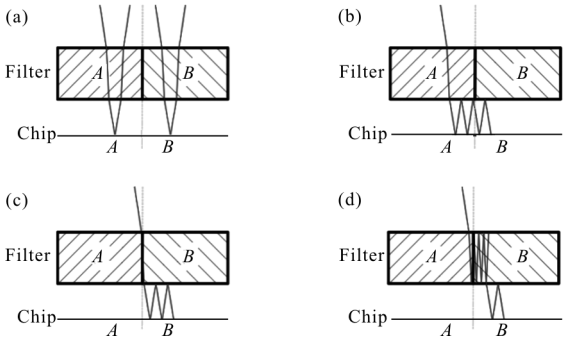

Fig.6 Several transmission path of the light after the filters

In order to eliminate the various factors described above that may cause stray light within the assembly, we have improved and controlled in the following aspects:

(1) Chip surface was designed to eliminate the interference, meantime reducing the substrate reflection area.

(2) The distance between the filter and the pixel was controlled.

(3) Low filter edge damage cutting method was used to keep fine filter edge.

(4) Critical surfaces were covered with infrared absorbing coating.

In order to evaluate the ability of the module to suppress stray light, a micro–spot measurement system was established to perform the stray light evaluation [5]. The block diagram of this system is shown in Fig.7. The blackbody is the radiation source, the blackbody radiation signal is modulated by the chopper, the modulated optical signal is irradiated through the optics and then irradiated on the detector pixels in the test Dewar. The pixels that receives the optical radiation signal generates the photoelectric signal. The signal is amplified by preamplifier and then read by the lock–in amplifier. As the stage moves, the

signals of the pixel at different positions can be obtained. The optical lens parameters of this system are shown in Tab.2.

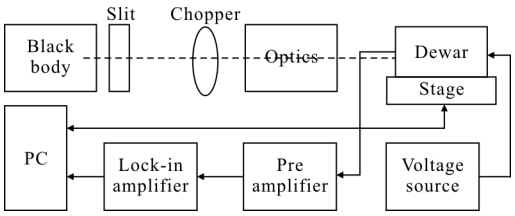

Fig.7 Schematic of micro-spot measurement system

Tab.2 Optical lens parameters of the micro-spot measurement system

Parameters	SWIR	MWIR	WVIR	LWIR
Wavelength/μm	2-3	3-5	5-8	8-13
F#	≤2	≤1.5	≤1.5	≤1.3
Focal length/mm	50	50	50	50
Field of view/mm^2	5×5	5×5	5×5	5×5
Diffuse spots/μm	15	20	30	30
Energy concentration	91%@ 30 μm	91%@ 30 μm	84%@ 30 μm	91%@ 56 μm
After work distance/ mm	≥20	≥20 m	≥0	≥20

The assemblies were tested using the micro-spot measurement system. Due to the problem of the MWIR lens, the response of the MS-A band was not tested. Figure 8 shows the response of the sensor in the three assemblies as the slit moves in the east-west (EW) direction. The response of the photovoltaic pixels in the test results is similar to that of Fig.9(a). The response result of the photoconductive pixel is similar to that of Fig.9(b). In Fig.9(a) there is an abnormal response on the left side of the pixels 1 and 2; similar response appears on the right side of the pixels 5 and 6. These are related to the detector chip structure, which corresponds to the area of the chip electrode hole shown in Fig.10.

It can be seen that there is no significant optical crosstalk outside the response area of the pixel and that the anti-stray measurement taken in the assembly is valid.

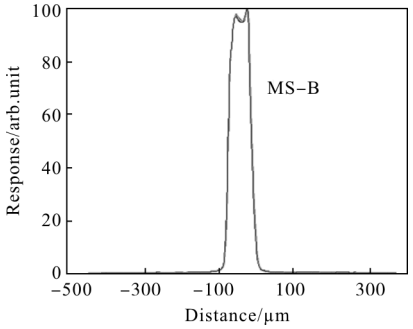

(a) MS-IR assembly

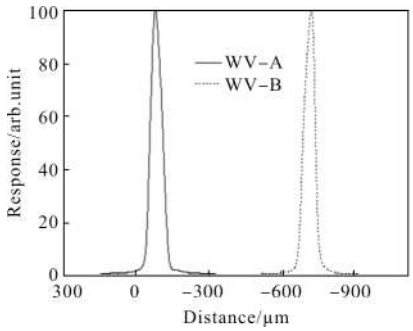

(b) WV-IR assembly

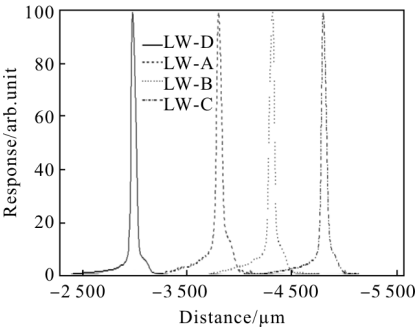

(c) LW-IR assembly

Fig.8 Relationship between detectors EW direction responses and position

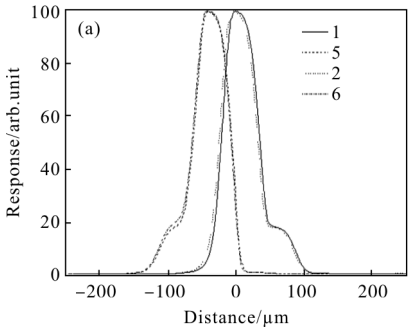

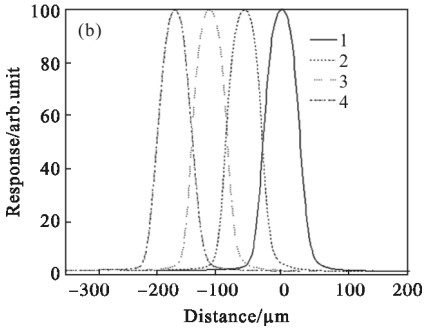

Fig.9 Relationship between detectors NS direction responses and position (a)PV chip (b)PC chip

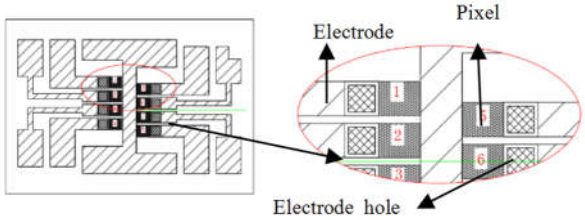

Fig.10 Layout of the PV chip

The MTF of the LW-IR pixel was tested. Test results showed that the MTF was greater than 0.5 in the EW direction and greater than 0.4 in the NS direction when the characteristic frequency was 8.93 lp/μm[6]. The results also demonstrate that the stray light suppression means of the assembly were effective.

3 Performance of the assemblies

The main perf ormances in infrared detector assembly include responsivity, noise, D^*, responsivity non-uniformity, and relative response spectra. Because D^* can avoid the influence of the detector area or the measurement bandwidth on the detector measurement results, it is often used to compare the advantages and disadvantages of the different detectors. D^* is calculated as[7]:

$$D^*=\sqrt{A_D}\cdot\sqrt{\Delta f}\cdot\frac{S_D}{\phi_s}\cdot\frac{1}{N_D}$$

Where Δf is the frequency bandwidth of the test system, S_D is the detector response signal, N_D is the detector output noise, and ϕ_s is the blackbody radiation energy.

The blackbody energy ϕ_s received by the detector under sinusoidal modulation is expressed as:

$$\phi_s=\frac{\sigma\cdot(T_b^4-T_0^4)A_b\cdot A_d}{2\sqrt{2}\,\pi L^2}$$

Where σ is the Storm-Boltzmann constant, is $5.669\ 7\times10^{-12}$ $(W\cdot cm^{-2}\cdot K^{-4})$; T_b is the black body temperature; T_0 is the ambient temperature; A_b is blackbody exit area; A_d is pixel area; L is test distance.

The responsivity non-uniformity U_R is a value of percentage that the mean square root of the pixels′ responses divided by the average response rate $\bar{R}$, as shown below:

$$U_R=\frac{1}{\bar{R}}\cdot\sqrt{\frac{1}{N}\cdot\sum_{i=1}^{N}\left[R_i-\bar{R}\right]^2}$$

Where N is the number of pixels in the same band, the value is 8 for the PV band, and 4 for the PC band.

Figure 11 is the blackbody performance test diagram for the infrared detectors. The blackbody is the infrared radiation source, after the modulation of the infrared radiation exposure to the detector pixels. Because of pixel′ s photoelectric effect, the photodiode produces a photo-generated current under the action of infrared radiation, and the conductance change signal in the photoconductive pixel. The signal is amplified by the preamplifier then to be input to the lock-in amplifier to obtain the amplitude of the signal. Table 3 is the electrical performance data for the detector assembly.

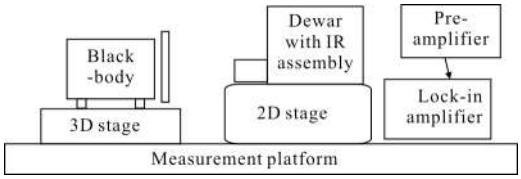

Fig.11 Schematic diagram of blackbody performance test system

Tab.3 Main electrical performance of the IR assemblies

Assembly	Wavelength /μm	Band symbol	Band center distance accuracy/ μm	D^*/cm·Hz$^{1/2}$·W^{-1}	Responsivity non-uniformity
MS-IR	2.1-2.35	MS-B	3-5	1.44×10^{12}-1.54×10^{12}	2.1%
	3.5-4.0	MS-A		1.21×10^{12}-1.33×10^{12}	2.9%
WV-IR	5.8-6.3	WV-B	5-10	9.14×10^{10}-10.7×10^{10}	6.3%
	6.9-7.3	WV-A		2.11×10^{11}-2.3×10^{11}	3.5%
LW-IR	8.0-9.0	LW-D	5-10	1.6×10^{11}-1.82×10^{11}	5.3%
	10.3-11.3	LW-C		1.01×10^{11}-1.15×10^{11}	7.8%
	11.5-12.5	LW-B		8.18×10^{10}-8.73×10^{10}	4.6%
	13.2-13.8	LW-A		5.62×10^{10}-6.88×10^{10}	6.0%

The relative response spectrum of the infrared detector assembly is quantitatively controlled, and Fig.12 is the control requirement for the spectrum of each band of the assembly. Table 4 shows the numberical values for ezch control point. The relative response spectrum shall be between the inner and outer line limits, and the area outside the required area shall not be greater than 3%.

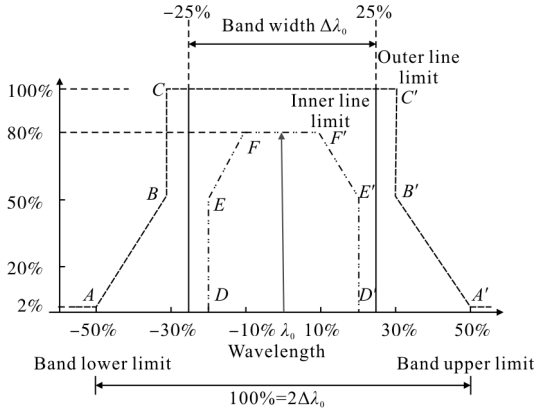

Fig.12 Requirement of the relative spectral response

Tab.4 Numberical values for each control point

Control point ($\lambda_{max}-\lambda_{min}=200\%\Delta\lambda_0$)						
	A/*A*′	*B*/*B*′	*C*/*C*′	*D*/*D*′	*E*/*E*′	*F*/*F*′
Band position	±50%	±30%	±30%	±20%	±20%	±20%
Weight	2%	50%	100%	0%	50%	80%

In order to achieve the assembly′s spectral quantitative control requirements, the filter and the chip spectrum need be screened. It is also necessary to consider the aspects of package design, surface treatment of the key parts, process control and so on.

Figure 13-15 are the relative spectral responses of the three assemblies, with a spectral response percentage less than 1% outside of the line limits.

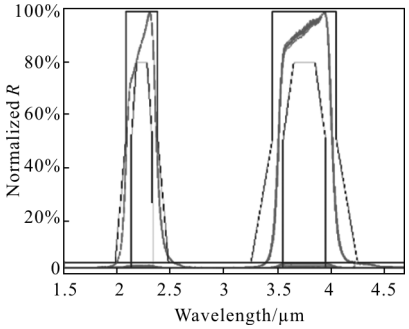

Fig.13 Relative spectral response of MS-IR assembly

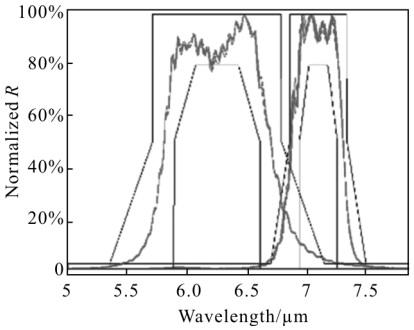

Fig.14 Relative spectral response of WV-IR assembly

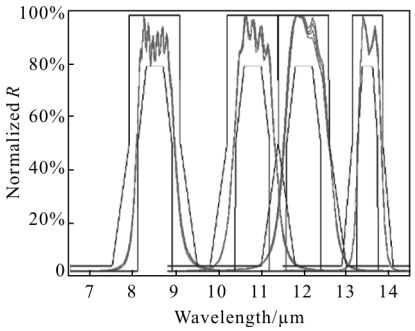

Fig.15 Relative spectral response of LW-IR assembly

4 Conclusion

This paper introduces the infrared detector assemblies used in the scanning radiometer. The radiometer has three infrared assemblies, covering

eight infrared channels. Three assemblies are integrated infrared chips, micro-filter, double lens and apertures. The assemblies were tested using the micro-spot measurement system. Experimental results showed that there had not significant optical crosstalk. The MTF of LW-IR was also evaluated, it was greater than 0.5 at the characteristic frequency of 8.93 lp/μm in the EW direction, and greater than 0.4 in the NS direction, which proved that the means of stray light suppression in the assembly were effective. The D^* of the MS-IR is greater than 1×10^{12}cm·Hz$^{1/2}$·W^{-1}, and the D^* of the LW-A channel is also better than 5.6×10^{10} cm·Hz$^{1/2}$·W^{-1}. The spec tra of the assemblies were quantitatively controlled, and the percentage of spectral responses outside the line limits was less than 1%.

References:

[1] Dong Yaohai. FY-4 meteorological satellite and its application prospect [J]. ***Aerospace Shanghai***, 2016, 33(2): 1-8. (in Chinese)

[2] Wang Ganquan, Chen Guilin. Two-dimensional scanning infrared imaging technology on geosynchronous orbit [J]. ***Infrared and Laser Engineering***, 2014, 43(2): 429-433. (in Chinese)

[3] Li Xinyao. Stray radiation investigating and suppressing of FY-2 [D]. Shanghai: Shanghai Institute of Technical Physics, Chinese Academy of Sciences, 2006. (in Chinese)

[4] Zhang Yan, Liu Dafu, He Xiangrong, et al. Stray light in infrared detector [C]//SPIE, 2009, 7383: 73831O.

[5] Wang Yang, Liu Dafu, Xu Qinfei, et al. Analysis on optical crosstalk of infrared photoconductive detector modules with different structures [J]. ***Infrared and Laser Engineering***, 2016, 45(4): 0404001. (in Chinese)

[6] Wang Yang, Liu Dafu, Xu Qingfei, et al. MTF of infrared detector modules with different structures [J]. ***J Infrared Millim Waves***, 2016, 35(3): 294-299. (in Chinese)

[7] Zhao Dingyuan, Mi Zhengyu. Introduction to Optoelectronic Devices [M]. Shanghai: Shanghai Scientific & Technological Literature Publishing House, 1989: 398-399. (in Chinese)